Nuclear Instruments and Methods in Physics Research A 792 (2015) 28–37

Contents lists available at ScienceDirect

Nuclear Instruments and Methods in Physics Research A

journal homepage: www.elsevier.com/locate/nima

# Development of a modular directional and spectral neutron detection system using solid-state detectors

A. Weltz *, B. Torres, L. McElwain, R. Dahal, J. Huang, I. Bhat, J. Lu, Y. Danon

*Rensselaer Polytechnic Institute, 110 8th St., Troy, NY 12180, USA*

ARTICLE INFO

*Article history:*
Received 5 January 2015
Received in revised form
22 April 2015
Accepted 23 April 2015
Available online 5 May 2015

*Keywords:*
Microstructured solid-state neutron detector
Directional and spectral neutron detection
Special nuclear material
MCNP

ABSTRACT

A detection system using room-temperature, microstructured solid-state thermal neutron detectors with very low leakage current has been developed at Rensselaer Polytechnic Institute (RPI) with the ability to provide positional and spectral information about an unknown neutron source. The Directional and Spectral Neutron Detection System (DSNDS) utilizes a set of small-but-scalable, zero-bias solid-state thermal neutron detectors which have demonstrated high thermal neutron efficiency and adequate gamma insensitivity. The DSNDS can gather spectral information about an unknown neutron source with a relatively small number of detectors, simplifying the detector electronics and minimizing cost; however, the DSNDS is modular in design, providing the capability to increase the detection efficiency and angular resolution. The system used in this paper was comprised of a stack of five high-density polyethylene (HDPE) disks with a thickness of 5 cm and a diameter of 30 cm, the middle disk containing 16 detectors positioned as one internal (moderated) and one external (unmoderated) ring of solid-state neutron detectors. These two detector rings provide the ability to determine the directionality of a neutron source. The system gathers spectral information about a neutron source in two ways: by measuring the relative responses of the internal ring of detectors as well as measuring the ratio of the internal-to-external detector responses. Experiments were performed with variable neutron spectra: a $^{252}$Cf spontaneous fission neutron source which was HDPE moderated, HDPE reflected, lead (Pb) shielded, and bare in order to benchmark the system for spectral sensitivity. Simulations were performed in order to characterize the neutron spectra corresponding to each of the source configurations and showed agreement with experimental measurements. The DSNDS demonstrates the ability to determine the relative angle of the source and the hardness of the neutron spectrum. By using the single HDPE disk with two detector rings and stacking four moderator disks, the intrinsic efficiency for $^{252}$Cf spectrum of such detector is about $0.4\% \pm 0.04\%$.



## 1. Introduction

Neutron detection is important for homeland security efforts, including monitoring national points of entry for the presence of special nuclear material (SNM), which is defined as plutonium and uranium enriched in $^{233}$U or $^{235}$U and is the fissile component of nuclear weapons [1]. Currently, neutron detection systems – such as radiation portal monitors (RPMs) – are implemented at U.S. borders, ports, airports etc. to screen vessels, vehicles, cargo, and individuals in order to thwart the illicit trafficking of SNM. The Domestic Nuclear Detection Office (DNDO) reports that in 2011 there were 444 RPMs operating at U.S. seaports, which were used by Customs and Border Protection (CBP) to screen approximately 24.3 million containers which entered the U.S. [2]. If an RPM alarm is triggered and confirmed during a screening, the container is diverted and the source has to be located within the vehicle or container (or identified as a false alarm). The thoroughness of such a process and high volume of traffic can cause delays at ports-of-entry [3]. The time used to survey shipping containers has an economic impact in U.S. trade. The implementation of the DSNDS can improve this process by providing spectral and improved directional information about the potential source, automating the process of hand-held surveying to locate a neutron source.

The "gold standard" of neutron detectors is the $^{3}$He proportional counter. These are robust, gamma insensitive, and remain an efficient, proven technology for detecting thermal neutrons [3]. However, a global shortage of $^{3}$He has caused the price to surge and limits the future supply of these neutron detectors, stimulating the development of alternative neutron detection technology. $BF_3$ proportional counters demonstrate adequate thermal neutron efficiency and gamma discrimination, but higher bias voltage requirements ( $>$ 2000 V depending on the gas pressure) and toxicity of the

* Corresponding author. Tel.: +1 2159083747.
*E-mail addresses:* weltza3@gmail.com, ltza@rpi.edu (A. Weltz).

http://dx.doi.org/10.1016/j.nima.2015.04.050
0168-9002/

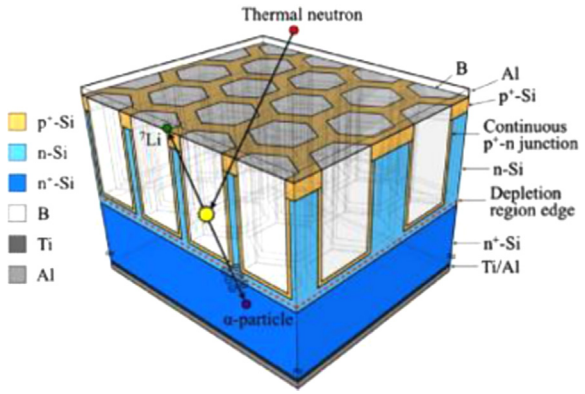


**Fig. 1.** Schematic of a honeycomb structured solid-state neutron detector [10].

gas require additional considerations before deploying devices in the field [4]. In contrast, the solid-state neutron detectors developed at RPI have a flat, compact geometry and require no bias voltage, allowing for the development of new neutron detection systems and improvements to existing technologies [5].

### 1.1. Solid-state neutron detectors

Microstructured solid-state neutron detectors have been developed by several groups [6–9]. The solid-state devices implemented for this system were fabricated within RPI's Micro and Nano Fabrication Clean Room using boron enriched to 93% $^{10}$B as the neutron converter which is deposited into deep, micron-sized hexagonal holes that are etched into a silicon wafer creating a microstructured honeycomb pattern, seen in Fig. 1 [10]. These devices have a unique passivation method that allows for very low leakage current and higher efficiency. It is estimated that these devices and the associated electronics in mass production will cost less than existing neutron detectors.

Neutrons are detected in a multi-step process beginning with the absorption of a moderated neutron by $^{10}$B within the hexagonal holes of the device. The $^{10}$B absorption reaction results in two energetic charged particles and is shown below:

$$^{10}_{5}\mathrm{B}+^{1}_{0}\mathrm{n}\rightarrow\{\,94\%:{}^{7}_{3}\mathrm{Li}\ (0.84\ \mathrm{MeV})+{}^{4}_{2}\alpha\ (1.47\ \mathrm{MeV})6\%:{}^{7}_{3}\mathrm{Li}\ (1.015\ \mathrm{MeV})+{}^{4}_{2}\alpha\ (1.777\ \mathrm{MeV}).$$

The resulting $^{7}$Li and $^{4}\alpha$ ions are emitted in opposite directions and can escape the boron entering the silicon region with a fraction of their initial energy. The remaining energy is deposited in the charge-collecting silicon, which is contacted with sputtered aluminum and titanium. Subsequent preamplification, pulse shaping, and discrimination of the signal from the RPI devices allow for neutron events to be identified if the pulse height is greater than the electronic noise and gamma background, which is measured at 200 keV [5].

These honeycomb detectors have demonstrated an intrinsic thermal neutron efficiency of up to 29%, a γ discrimination ratio better than the PNNL recommendation for a well-designed neutron detector ($10^{-6}$ for a 10 mR/h exposure rate from a $^{60}$Co source), and scalability to large surface areas due to an extremely low leakage current [5,10,11]. Solid-state neutron detectors – as opposed to their gas-filled counterparts – are flat, compact, require no bias voltage, and are thus easier to embed in different moderated configurations.

### 1.2. Existing directional and spectral neutron detection systems

The DSNDS utilizes the concept of embedding thermal detectors in moderators, which is not new [12–15]. There have been many iterations of neutron rem counters, which consist of a thermal neutron detector placed inside a moderator such that the instrument's energy-dependent response is proportional to the neutron flux-to-dose conversion over a wide energy range. Bonner spheres, which consist of a thermal neutron detector surrounded by spherical moderators of different sizes, were designed in 1960 in order to measure the neutron dose rate from thermal energy to 15 MeV within ±50% [16]. In 1964 Andersson and Braun published and developed the A–B rem counter, which consists of a central $BF_3$ proportional counter surrounded by two cylinders of polyethylene separated by borated plastic which serves to absorb low-energy neutrons. The borated plastic layer suppresses the instrument's response to thermal neutrons to nearly zero, but this sensitivity was increased by drilling holes in the borated plastic. The size and number of holes can be controlled to produce a thermal neutron response which matches the ideal rem response. This instrument provides an improved rem-proportional response for energies between 0.0253 eV and 10 MeV [17]. Leake contributed to neutron rem counters by creating a spherical version of Andersson and Braun's design, which utilized cadmium (Cd) instead of borated polyethylene. This instrument is smaller and lighter (originally 6.5 kg including electronics), which proved useful as a portable neutron rem counter [18]. There has been an effort to extend the range of neutron rem counters to higher neutron energies. The Long Interval NeUtron Survey meter (LINUS) – an adaptation of the A–B rem counter – was developed in order to achieve a flat response from 1 MeV up to several hundred MeV [19]. The LINUS was created from an A–B rem counter and a 1-cm-thick layer of Pb, which surrounds the neutron absorption layer. Neutrons with energy greater than 10 MeV undergo inelastic scattering in the Pb layer, which are moderated by the polyethylene and detected by the internal $BF_3$ proportional counter. There is no significant effect on neutrons with energy below 10 MeV, so the LINUS achieves increased sensitivity to neutrons with energy greater than 10 MeV, while remaining an accurate rem counter for neutrons with energy below 10 MeV [20,21]. The DSNDS is similar in principle and design – excluding the absence of a central detector – to the aforementioned instruments but differs in purpose. The aforementioned instruments provide a response to neutrons over a wide energy range which is proportional to the ideal rem response curve; however, the application described here does not measure the neutron dose. The DSNDS provides directional and spectral information about a neutron source for the purpose of identifying its location.

A previous version of a portable directional neutron detection system was developed by Schulte et al. with thin-films of gadolinium converter foils between silicon detectors [12]. The angular orientation of the detectors allows for the system to determine the most likely direction of a neutron emitting source. However, these detectors are gamma sensitive, requiring additional modules for gamma compensation; additionally, this system lacks sufficient angular resolution. Other portable directional neutron source finders have since been developed using $^{6}$Li glass scintillators or $^{3}$He detectors embedded in polyethylene moderators [15]. Most recently, Caruso et al. patented a spectral and directional neutron apparatus using a plurality of solid-state detectors embedded in a moderator [14]. In reference, spectral information is obtained by embedding detectors at different depths in the moderator designed to create different sensitivities to the neutron spectrum.

The DSNDS is distinguished by the utilization of the aforementioned solid-state neutron detectors developed at RPI, the modularity of the system, and the method by which neutron spectral information is obtained. The DSNDS utilizes a cylindrical moderator with an internal and external ring of detectors separated by a neutron absorber. The annular distribution of the internal detectors within the DSNDS serves two purposes: to determine the source directionality and to provide measurements with incremental effective moderator thicknesses. The shape of the angular detector responses are used to gather additional spectral information. Lastly,

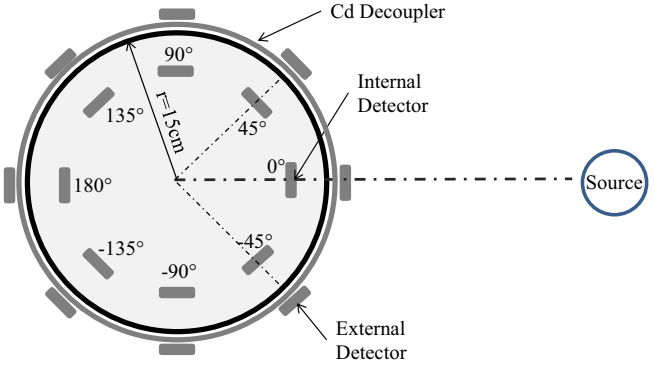


**Fig. 2.** DSNDS schematic demonstrating the source and detector positions within the HDPE including a neutron decoupler.

the modularity of the DSNDS allows for the customization of the instrument based upon a tradeoff of improved efficiency and angular resolution contrasted with low cost and simplified detector electronics. Increased detection efficiency for fast neutrons can be attained by embedding more detectors into the 5-cm-thick disk and stacking several such disks to increase the detection area.

## 2. Design considerations

The DSNDS concept was designed in order to determine the spectral properties and position of a neutron source. A diagram showing the DSNDS can be seen in Fig. 2, where the eight internal and eight external detectors are secured in a ring around the center of the HDPE disk, as discussed in Section 1. The solid-state neutron detectors used in the DSNDS each have an area of 4 $cm^2$. These devices are thermal neutron detectors, thus fast neutrons must be moderated in order to be efficiently detected by this system.

The DSNDS cylinder is composed of five stacked HDPE disks, each with a height of 5 cm and a radius of 15 cm. Stacking the disks to make a cylinder provides modularity. Only the middle disk contains the rings of detectors (the other four disks serve only as neutron moderators); however, this stacked design can be made more efficient by replacing the moderating disks with additional detector disks. Additionally, the efficiency and angular resolution of the DSNDS can be improved by increasing the number of detectors that compose the internal ring or by adding additional detector rings.

The annular arrangement of the internal detectors within the DSNDS provides variable thicknesses of HDPE moderation for a given source position. These detectors with incremental effective moderation provide relative responses which are characteristic of the neutron spectrum incident on the DSNDS.

The external detectors shown in Fig. 2 were designed to have no moderation between the source and detectors such that they are sensitive to incident thermal neutrons and, to a lesser extent, higher energy neutrons. The sensitivity of the detectors diminishes with increasing energy due to the cross-section of the $^{10}B$ neutron converting material which varies with $1/\sqrt{E}$. Conversely, the internal detectors are moderated by at least 3.5 cm of HDPE on the front and much larger HDPE thickness behind the detector, which enables them to effectively detect fast neutrons incident on the DSNDS. This design allows for the DSNDS to collect spectral information about a neutron source in two ways: using the ratio of the internal-to-external detector response and the distribution of count rates of the internal ring of detectors.

A Cd layer (or possibly another thermal neutron absorber) surrounds the cylinder separating the internal and external detector rings, which serves to decouple the thermal neutron response of the two rings of detectors. The Cd wrapped around the cylinder absorbs neutrons below the Cd cutoff (0.5 eV) which were moderated by the cylinder, preventing low energy neutrons from scattering back into the external detectors, effectively decoupling the thermal neutron response of the internal and external detectors. Cd, which is a toxic metal, is not essential to the design. Alternative neutron absorbers – e.g. gadolinium or boron – are also effective decouplers.

### 2.1. Design optimization

The DSNDS, which is housed in a cylinder of HDPE ($\rho = 0.94$ g/$cm^3$), was simulated using Monte Carlo N-Particle Code (MCNP) 6.1 [22] in order to determine the appropriate dimensions of the system. Since the solid-state detectors respond to thermal neutrons, the internal detectors should be positioned where the thermal neutron flux peaks due to an incident fission neutron spectrum. This optimal radial position of the internal detectors was determined by simulating a typical fission neutron spectrum and tallying the $^{10}B$ neutron absorption rate at different radii inside the HDPE cylinder with a radius of 15 cm and height of 25 cm. The results of this simulation, which were run until $2 \times 10^7$ histories were completed, show that the internal detectors should be positioned at a radius which is about 3.5 cm smaller than the radius of the cylinder, as seen in Fig. 3a.

Since the DSNDS is designed to be modular, simulations were performed in order to investigate the effect of the cylindrical height and radius. First, the height of the large HDPE cylinder was varied in order to investigate how changes in the cylindrical height affect the response of the internal detectors at the optimal radius. The results of these simulations can be seen in Fig. 3b, which are displayed as a relative response compared to the effectively infinite cylinder. This simulation demonstrated that a height of 25 cm provides enough neutron moderation to achieve a detector response which is $>99\%$ of the response associated with the effectively infinite cylinder.

Similarly, the radius of the cylinder was varied in order to determine the response of the internal detectors as a function of the cylindrical radius. Fig. 3c shows that a cylindrical radius of 15 cm provides enough moderation to achieve an internal detector response which is $>95\%$ of the response associated with an effectively infinite cylinder.

The system fabricated for the laboratory experiments has a radius of 15 cm, a height of 25.4 cm, a detector angular spacing of 45°, and a hole in the center of the moderating cylinder—seen in Fig. 4b. As constructed, the DSNDS – including 16 detectors – has a mass of about 16 kg. The central hole was used to house the $^{252}Cf$ source during detector calibration, a process to determine the relative detector efficiencies in order to normalize the individual detector responses. This hole can be plugged if needed. The system is shown in Fig. 4 with 8 (4 internal and 4 external) of the 16 total detectors.

### 2.2. Efficiency determination

The intrinsic efficiency of the DSNDS is defined as the probability of detecting a neutron which is incident on the cylinder and was calculated for the bare (unmoderated) $^{252}Cf$ source. The strength of the $^{252}Cf$ source was calibrated as 0.5 mCi ($\pm 10\%$) on the third of September of 2009. Considering the source half-life of 2.646 years, the probability of spontaneous fission (3.1%), and the average number of neutrons emitted per fission event (3.73), the source intensity during the experiments was calculated to be 0.13 mCi or $2.39 \times 10^6$ n/s ($\pm 10\%$) [23].

Experimental measurements utilized an ORTEC 142AH preamplifier, an ORTEC 672 Spectroscopy amplifier, and ORTEC MAESTRO Multi-Channel Analyzer (MCA) software in order to record the detector responses. The intrinsic efficiency of the 0° internal detector was measured to be $0.07\% \pm 0.01\%$, which is defined as the probability of neutron detection given a neutron is incident on the HDPE cylinder (height = 25.4 cm, radius = 15 cm). Similarly, the

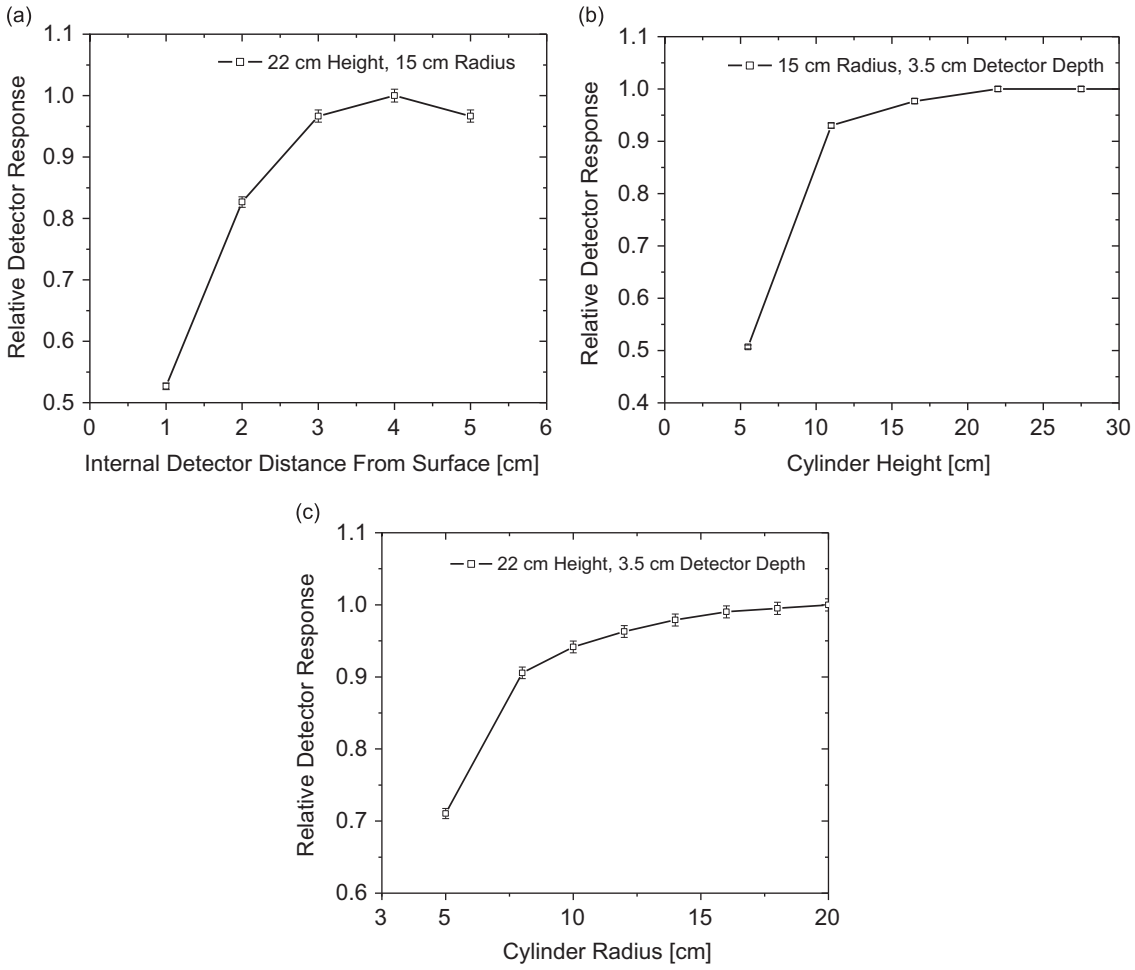


**Fig. 3.** MCNP-simulated detector responses used to optimize the system's dimensions. (a) Was used to determine the internal detector location ($r=11.5$ cm), (b) the cylinder height (15 cm), and (c) the cylinder radius (15 cm).

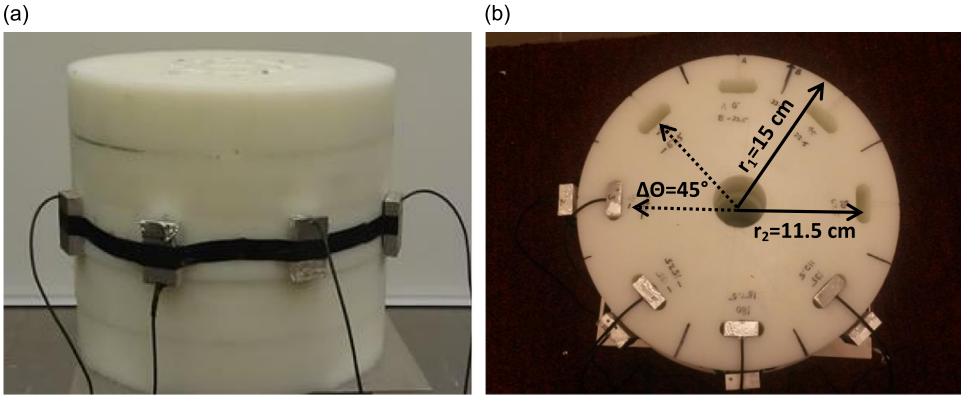


**Fig. 4.** (a) Front view of the system showing the external ring of detectors mounted on 5.08 cm (2″) thick center HDPE disk, (b) top view of the system showing four internal and four external detectors.

efficiency of the system with $16\times4$ cm$^2$ detectors – comprised of one internal and one external ring of detectors – was determined to be $0.43\pm0.04\%$ using the collected detector count rates, the neutron emission rate of the $^{252}$Cf source, and the solid angle of the cylindrical moderator corresponding to the distance between the source and the cylinder and the area of the cylinder. Although the intrinsic thermal neutron efficiency of each device is as high as 29%, the low intrinsic efficiency of the DSNDS reflects its dependence on the moderation process.

MCNP simulations, which modeled the source-detector distance of 1.15 m and included the concrete walls and floor of the laboratory, were performed in order to imitate the experimental measurements until $10^8$ histories were completed. The responses of the microstructured solid-state detectors within the HDPE cylinder were modeled using a repeated structure of 3 μm hexagonal holes filled with enriched (93%) $^{10}$B ($\rho=2.35$ g/cm$^3$) embedded in Si, which were modeled after the geometry shown in Fig. 1. The simulations were used to verify that the efficiency of the

0° detector is about 0.07% ± 0.01%, with uncertainty due to simulation statistics and uncertainty in the original source calibration. Similarly, the overall detection efficiency of the DSNDS with all 16 detectors to a fission neutron source is 0.4% ± 0.1%. Additional simulations were performed with incremental, monoenergetic neutron sources in order to verify that the total intrinsic efficiency of the DSNDS increases with softer incident neutron spectra. Thus, the intrinsic efficiency measurements with the bare $^{252}$Cf source are conservative.

The lower level of detection (LLD) of these solid-state thermal neutron detectors was previously determined by measuring the pulse height spectrum corresponding to a moderated $^{252}$Cf source [5]. The energy of the highest pulse was equated to 2.79 MeV, which is the sum of the $^{4}\alpha$ and $^{7}$Li daughter ion energies corresponding to the more energetic $^{10}$B absorption reaction. This calibration was used to determine that the energy associated with the noise level of the measured spectrum is 200 keV. Therefore, in the simulations it was assumed that at least 200 keV of energy deposition in the silicon region of the detector is required for a neutron to be detected.

The efficiency of the DSNDS to fast neutrons can be further improved by increasing the area of the internal thermal neutron detectors. For example, the internal ring of detectors could be replaced with a solid ring of detectors with the same radius of 11.5 cm. The ring could be pixelated into 36 elements each with an area of $2 \times 4$ cm$^2$ and a total detection area of 288 cm$^2$. This ring would reduce the angular spacing of the detectors to 10°, improving the angular resolution. MCNP simulations, which agreed with measurements for a single detector and a system of 16 detectors, determined that the detection ring would provide an intrinsic efficiency of 1.25%. Implementing these rings in each of the 5 stacked disks would increase the effective detection area by a factor of about 5, and simulations estimate that this configuration would increase the intrinsic efficiency to 4.6%.

## 3. Experiments with different neutron spectra

Experiments performed at RPI aimed to demonstrate that the DSNDS can achieve the desired design goals of determining the relative angle of the source location and collecting information about the energy spectrum of an unknown neutron source. The experimental configuration is represented by Fig. 5, where RPI's DSNDS was positioned along with a $^{252}$Cf source, which was suspended in the laboratory in one of three configurations: bare (no moderator), reflected, and moderated, which were created using a 5.08 cm (1″) HDPE disk as a moderator and reflector. These three source configurations result in neutron spectra with decreasing fractions of fast neutrons. After these three measurements were performed and an empirical relationship was formed, a fourth spectrum was created in order to test the system's ability to measure an unknown neutron spectrum. The test source configuration was created by moderating the $^{252}$Cf source with 1.27 cm (0.5″) of HDPE. A final experiment was performed with a 5-cm Pb shield in front of the source in order to investigate the effect of a high-$Z$ shield on the neutron spectrum.

Each of the aforementioned measurements was performed with the source positioned 1.15 m away from the cylinder, aligned axially and laterally with the 0° detector. This source-detector distance was chosen to represent a survey measurement taken in a real-world situation, e.g. within a shipping container. The source-detector distance does affect the response of the DSNDS; for instance, increasing the distance increases the contribution of scattered neutrons from the surroundings, resulting in softer measured neutron spectra. This effect is difficult to account for because the DSNDS is sensitive to externally-scattered neutrons and it should be considered when interpreting the spectral results of the DSNDS. Additionally, when the distance between the source and the DSNDS is small, the external detectors become significantly closer to the source than the internal detectors, overestimating the hardness of the source. MCNP 6.1 simulations verified that the DSNDS will perform as designed when the source-detector distance is greater than 0.5 m.

Measurements performed with the DSNDS for the purpose of this paper included a single detection disk (one internal and one external ring) and were not designed to investigate the system's ability to determine the relative height of a neutron source. However, MCNP simulations verify that varying the height of the source from $z=-1.0$ m to $z=1.0$ m doesn't change the calculated two-dimensional angle or hardness of the source spectrum when the source-detector distance is $>0.5$ m. Changing the height will decrease the absolute count rate due to the small solid-angle, which can be overcome by a longer counting time. Stacking multiple detection disks would provide the ability to gather information and quantify the relative height of the neutron source in a similar fashion to the method of determining the two-dimensional angle proposed in the subsequent section.

### 3.1. Determination of the source spectrum

The neutron energy spectra of the three initial experimental source configurations were simulated with MCNP6.1 using a typical fission neutron energy spectrum. The MCNP inputs included the surrounding features of the laboratory, i.e. the concrete walls and floor, in order to represent external neutron scattering. The three source spectra represented in Fig. 6 were used to determine the fast neutron factor (FNF), which is defined as the fraction of neutrons above 1.0 eV, as seen in Table 1. The cutoff of 1.0 eV was chosen in order to effectively separate the neutron spectrum into two regions: the fast neutron region where neutrons are not fully moderated and the thermal neutron region where the neutron energy is defined by the Maxwell–Boltzmann distribution. The response of the DSNDS to the three characterized neutron spectra was used as a benchmark to characterize the system.

The measured responses of the internal detectors were normalized to the 0° detector and are plotted as a function of the detector angular position in Fig. 7.

The moderated source configuration has the softest energy spectrum and results in the narrowest distribution. Conversely, the bare source has the hardest spectrum and results in the broadest angular distribution. The reflected source, which has an intermediate spectrum, has a shape which lies between the moderated and bare source configurations, evident in Fig. 7. The normalized internal detector responses from Fig. 7 were characterized by measuring the full width at half maximum (FWHM), which are shown in Table 2. This parameter provides useful information about the incident source spectrum; however, the distribution cannot be created immediately, as it requires statistically significant counts from multiple detectors. The measurements shown in Fig. 7 were collected for 300 s with a distance of 1.15 m between the DSNDS and the $^{252}$Cf source, resulting in 3650 counts by the 0° internal detector and an average of 2410 counts by the five highest-counting detectors (located at ±90°, ±45°, and 0°). The uncertainty of the measurements assumes Gaussian statistics, where the standard error is the square root of the counts for each data point.

A calculation was performed in order to determine the count time required to achieve an average uncertainty of $<15\%$ for each of the five detectors located at ±90°, ±45°, and 0° when the system is deployed 1.15 m from a given sample of SNM. Arbitrarily, a sample of 0.5 kg of weapons grade plutonium (93% $^{239}$Pu and 7% $^{240}$Pu) was chosen, which has a neutron emission rate of $3.6 \times 10^4$ n/s due to the spontaneous fission of $^{239}$Pu and $^{240}$Pu [23]. Based upon the count rates measured with the $^{252}$Cf source

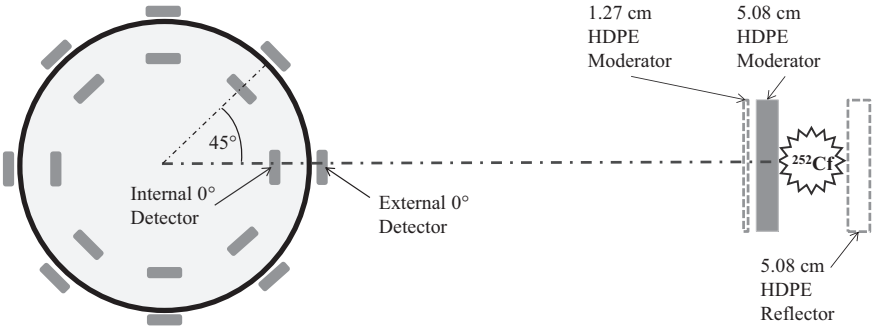


**Fig. 5.** Experimental configuration used to represent laboratory experiments where the $^{252}$Cf source was aligned with the 0° detectors of the DSNDS in one of four different source configurations: bare, moderated (5.08 cm HDPE), lightly moderated (1.27 cm HDPE), or reflected.

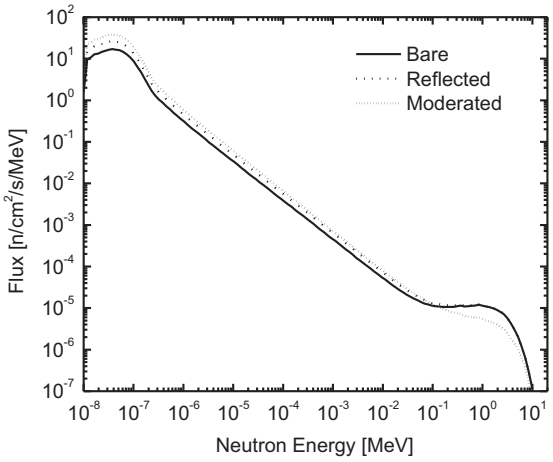


**Fig. 6.** MCNP-simulated neutron flux per source neutron incident on the DSNDS corresponding to three $^{252}$Cf source configurations.

**Table 1**
Three source configurations characterized by the FNF: the fraction of neutrons above 1 eV.

| *Source* | FNF ( > 1.0 eV) |
|---|---|
| Bare | 0.95 |
| Reflected | 0.93 |
| Moderated | 0.85 |

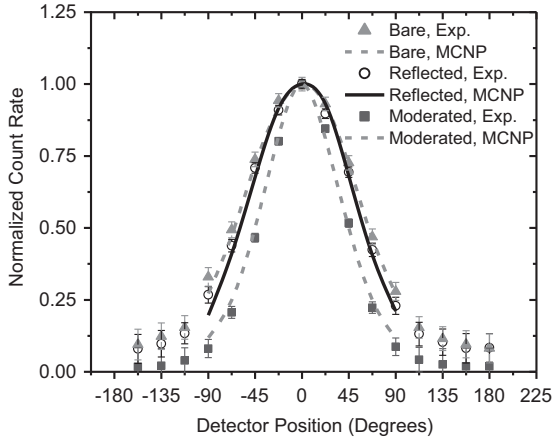


**Fig. 7.** Experimental and MCNP-simulated distribution of the relative count rates of the internal ring of detectors corresponding to three source spectra.

and the relative strength of the arbitrary Pu sample, a measurement time of 830 s (13.8 min) would be required to achieve an uncertainty of $<15\%$ for each the five detectors between $-90°$ and 90°.

**Table 2**
Simulated fast neutron factor (FNF) for three source configurations and the associated measured FWHM of the detector system's normalized response and the internal-to-external detector ratios with and without the Cd decoupler.

| *Source* | FNF | FWHM [°] | Internal-to-external ratio with Cd | Ratio without Cd decoupler |
|---|---|---|---|---|
| Bare $^{252}$Cf | 0.95 | $132 \pm 4$ | $26.1 \pm 1.1$ | $5.8 \pm 0.5$ |
| Reflected $^{252}$Cf | 0.93 | $110 \pm 4$ | $11.9 \pm 0.3$ | $4.1 \pm 0.4$ |
| Moderated $^{252}$Cf | 0.85 | $89 \pm 4$ | $7.3 \pm 0.2$ | $1.2 \pm 0.2$ |

A second spectral measurement involving the internal and external detectors was performed in order to provide a more immediate analysis for real-time surveys. The internal-to-external ratio was calculated by dividing the summed response of the internal detectors by the summed response of the external detectors. The measured ratios of the internal-to-external detector responses with and without a Cd decoupler are shown in Table 2, along with the simulated FNF and the measured FWHM. The use of a Cd decoupler improves the system's sensitivity to variations in the hardness of the neutron spectrum. The FWHM for the three sources is shown in Fig. 8a, and the internal-to-external ratio corresponding to the three sources is depicted in Fig. 8b. The steep increase in the measured parameters (FWHM and Internal-to-External Ratio) above a FNF of 0.94 shows the sensitivity of the system to small changes in the neutron spectrum in this region; however, additional data would produce a smoother curve and provide a more accurate spectral quantification for an unknown neutron source.

A fourth neutron spectrum was measured with the DSNDS in order to test the sensitivity of the DSNDS to small changes in the neutron spectra and simulate the process of measuring an unidentified source. The measurement was performed with a Cd sheet surrounding the DSNDS in similar fashion to the three benchmark experiments. This test source configuration was created by moderating the $^{252}$Cf source with a large, 1.27 cm (0.5″)-thick HDPE sheet (Fig. 5). The FNF of this neutron spectrum was determined by MCNP simulation to be 0.94. This spectrum has a FNF which lies between the bare $^{252}$Cf and reflected $^{252}$Cf source configuration (0.95 and 0.93, respectively); the simulated neutron spectra of the test source configuration and bare source configuration are shown in Fig. 9.

The response of the internal detectors of the DSNDS corresponding to the test source configuration can be seen in Fig. 10. This configuration yields a FWHM of $126 \pm 4°$ and an Internal-to-External ratio of $15.1 \pm 0.2$; both fall between the bare $^{252}$Cf source and the reflected $^{252}$Cf source. The empirical relationships created by the three original source configurations shown in Fig. 8 were interpolated in order to quantify the FNF using the FWHM and Internal-to-External ratio measured from the DSNDS. The results

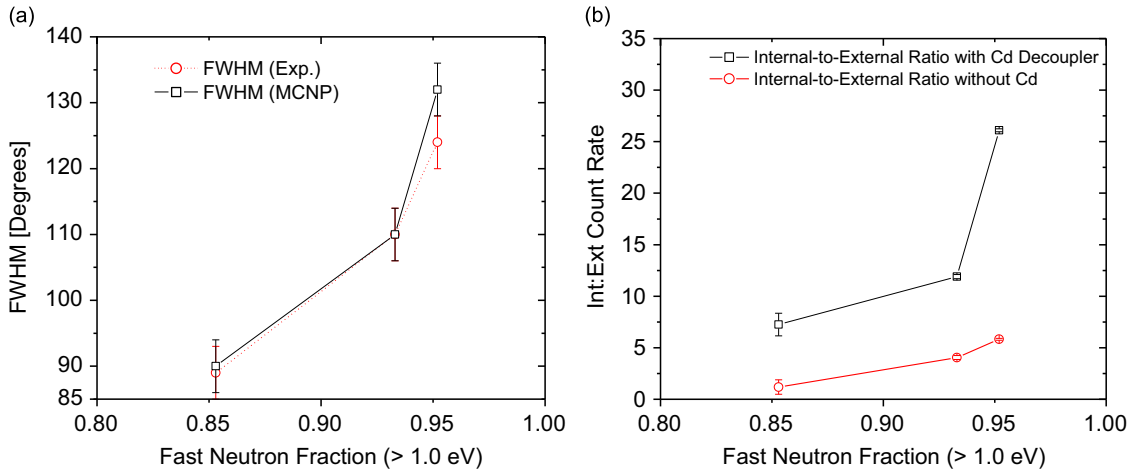


**Fig. 8.** Empirical relationship between (a) the measured FWHM and FNF and (b) the measured Internal-to-External ratio and FNF.

are shown in Table 3, which demonstrates the relationship between the FNF determined by MCNP simulation and the Internal-to-External ratio and FWHM.

These results demonstrate that the DSNDS is sensitive to small changes in a neutron energy spectrum by the determination of the FWHM and Internal-to-External ratio. Additionally, the information provided by the DSNDS can be used to determine the FNF of an unknown neutron spectrum by the interpolation of an empirical relationship created from measurements with multiple known neutron spectra. Determining the FNF of a source using the DSNDS provides information about a potentially hidden neutron source. For instance, a large FWHM confirms that the source has a fast neutron fraction near unity, which indicates that a neutron source is relatively unmoderated. Conversely, a smaller fast neutron fraction indicates that a source is moderated.

An additional experiment was performed in order to investigate the effect of shielding a neutron source with a high-Z material. This experiment models the scenario where a sample of diverted SNM is shielded to prevent the discovery of the diverted material by gamma detection. This source configuration involved shielding the $^{252}$Cf source with a 5-cm-thick Pb slab. The simulated spectrum corresponding to this configuration is normalized and compared to the bare $^{252}$Cf source spectrum and can be seen Fig. 11.

The Pb-shielded spectrum is nearly indistinguishable to the bare $^{252}$Cf source spectrum. The FNF was determined from the spectrum in Fig. 11 to be 0.95. The FWHM and Internal-to-External ratio were determined experimentally, and Table 4 shows a comparison of the Pb-shielded source and the bare source spectra and the DSNDS-measured parameters. As expected, the Pb-shielded source results in similar values for the FWHM and Internal-to-External ratio since high-Z materials are poor neutron moderators.

### 3.2. Determination of two-dimensional source angle

The data collected from the DSNDS can be used to determine the angle between the detector system and the source, which can be used in order to determine the location of a hidden neutron source. The angle is determined by first identifying the detector with the greatest calibrated count rate; the angular position of this detector and its associated count rate are denoted $\Theta$ and $R(\Theta)$, respectively. Similarly, the detectors adjacent to $\Theta$ are termed $\Theta+\Delta\Theta$ and $\Theta-\Delta\Theta$, where $\Delta\Theta$ is the angular spacing between adjacent detectors. A linear interpolation given in Eq. (1) was performed on the normalized count rates to approximate the source angle corresponding to the peak of the count rate distribution. This angle indicates the direction of the neutron source. The linear interpolation uses the normalized count rates of the detectors adjacent to the detector with maximum count

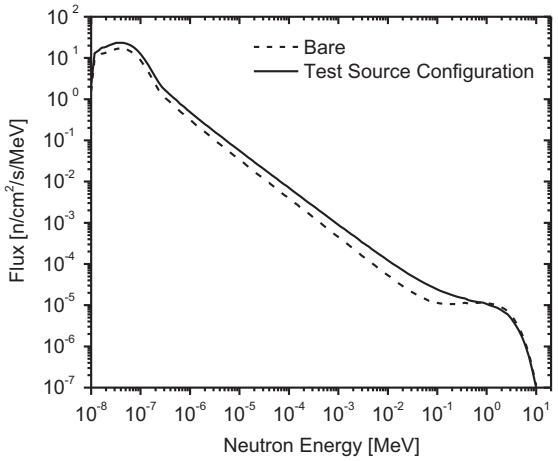


**Fig. 9.** MCNP-simulated neutron flux per source neutron incident on the DSNDS corresponding to the bare source configuration and the test source configuration in which a $^{252}$Cf source was moderated by 0.5″ of HDPE.

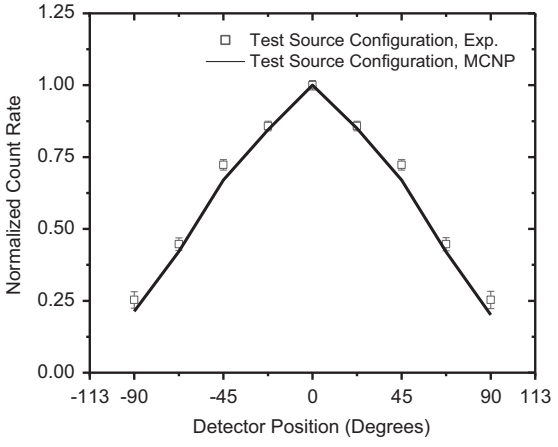


**Fig. 10.** Experimental and simulated distribution of the relative count rates of the internal ring of detectors corresponding to the test source configuration.

rate, $R(\Theta)$, which are denoted as $R(\Theta+\Delta\Theta)$ and $R(\Theta-\Delta\Theta)$.

$$\text{Angle}[^\circ] = \frac{R(\Theta+\Delta\Theta)-R(\Theta-\Delta\Theta)}{2-[R(\Theta+\Delta\Theta)+R(\Theta-\Delta\Theta)]} * \frac{\Delta\Theta[^\circ]}{2} + \Theta[^\circ] \quad (1)$$

**Table 3**
DSNDS response to a test neutron source configuration.

| *Source* | Simulated FNF | Measured FWHM [°] | Interpreted FNF from Fig. 8a | Measured internal to external ratio | Interpreted FNF from Fig. 8b |
|---|---|---|---|---|---|
| Test | 0.94 | 126 ± 4 | 0.94 | 15.1 ± 0.2 | 0.94 |

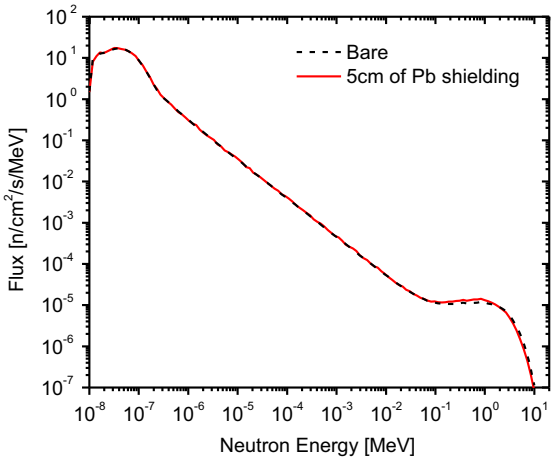


**Fig. 11.** MCNP-simulated neutron flux per source neutron incident on the DSNDS corresponding to the $^{252}$Cf source shielded with 5 cm of Pb, which is compared to the bare $^{252}$Cf neutron spectrum.

### 3.2.1. Angular resolution

The angular resolution of the system is dependent on the incident neutron spectrum, the angular spacing of the detectors, the counting statistics of the system, and the empirical model used to quantify the angle. The angular resolution is impacted by the incident neutron spectrum because the spectral hardness affects the width of the distribution of the internal detectors' relative responses, as discussed in Section 3.1 and seen in Fig. 7. The wider distribution corresponding to a hard neutron spectrum will have a poorer angular resolution than the narrower distribution of a soft neutron spectrum. The angular spacing of the detectors in this system is 45°, but additional detectors could be used to reduce the spacing. Additional detection disks could also be stacked and offset by an angle of $\Delta\Theta/n$, where $n$ is the number of stacked disks, to improve the angular resolution of the DSNDS. The counting statistics of the system depend on the strength of the neutron source, the distance between the source and the DSNDS, the efficiency of the system, and the counting time.

Previous Monte Carlo simulations using MCNP6.1 modeled three source configurations of a fission neutron source at a distance of 1.15 m, aligned axially with the 0° detector. These simulations were described in detail in Section 3.1, which demonstrated agreement with the experimentally-measured detector responses shown in Fig. 7. The MCNP6.1 input files corresponding to the bare and moderated source configurations were used to model an internal ring of sixteen detectors with a symmetric angular spacing of 22.5°. Since the internal ring of detectors is symmetric, a shift in the distributed detector responses by 22.5° simulates a change in the source position of the same angle. These simulations were used to demonstrate the sensitivity of the DSNDS to a change in the relative source angle for the bare and moderated neutron source configuration and can be seen in Fig. 12. The simulations were run with $10^8$ histories with the source modeled 1.15 m from the DSNDS, which results in a maximum relative uncertainty of 5% for the five detectors between −90° and 90°.

In order to demonstrate the resolution of the DSNDS in a real-world scenario, the uncertainty of each detector response was calculated corresponding to the neutron emission of the SNM

**Table 4**
Comparison of Pb-shielded and bare $^{252}$Cf source spectra and DSNDS-measured FWHM and internal-to-external ratio with the Cd decoupler.

| *Source* | Simulated FNF | Measured FWHM [°] | Measured internal-to-external ratio with Cd decoupler | Interpreted FNF from Fig. 8a | Interpreted FNF from Fig. 8b |
|---|---|---|---|---|---|
| Bare $^{252}$Cf | 0.95 | 132 ± 4 | 26.1 ± 1.1 | 0.95 | 0.95 |
| Pb-shielded $^{252}$Cf | 0.95 | 130 ± 4 | 25.4 ± 1.3 | 0.95 | 0.95 |

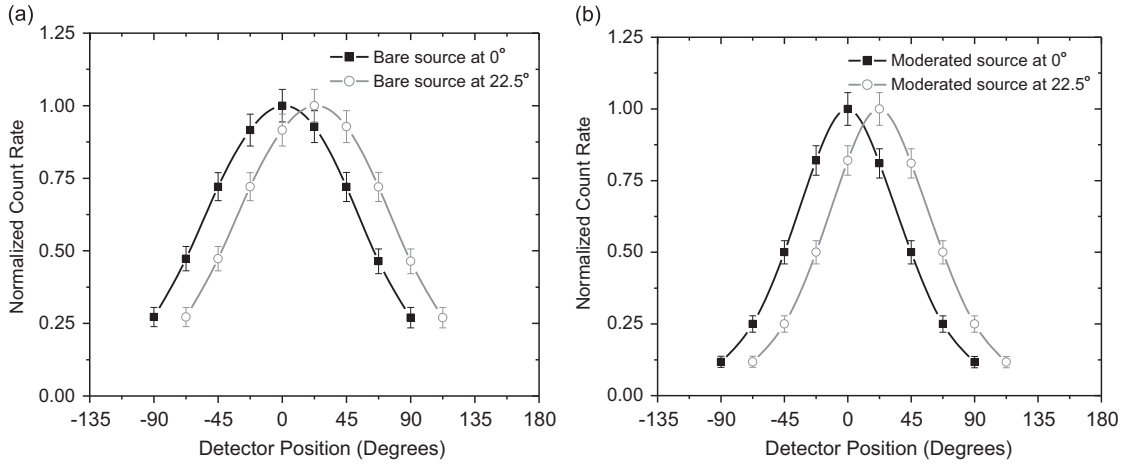


**Fig. 12.** MCNP simulations demonstrating the sensitivity of the DSNDS to a 22.5° shift in the source angle with error bars corresponding to the $^{252}$Cf source emitting $3 \times 10^7$ n at the 1.15 m position for: (a) the bare $^{252}$Cf source and (b) the $^{252}$Cf source moderated by 5 cm of HDPE.

**Table 5**
Tabulated results of the normalized, MCNP6.1-simulated internal detector responses used to determine the relative source angle using the linear interpolation of Eq. (1) and uncertainties corresponding to $3 \times 10^7$ emitted neutrons 1.15 m from the DSNDS.

| Bare source at 1.15 m and 22.5° | | | Moderated source at 1.15 m and 22.5° | | |
|---|---|---|---|---|---|
| Detector angle [°] | Uncertainties for SNM sample ($3 \times 10^7$ neutrons) | Uncertainties for $^{252}$Cf source ($7.2 \times 10^8$ neutrons) | Detector angle [°] | Uncertainties for SNM sample ($3 \times 10^7$ neutrons) | Uncertainties for $^{252}$Cf source ($7.2 \times 10^8$ neutrons) |
| −45 | $0.47 \pm 0.06$ | $0.47 \pm 0.01$ | −45 | $0.25 \pm 0.05$ | $0.25 \pm 0.01$ |
| 0 | $0.92 \pm 0.08$ | $0.92 \pm 0.02$ | 0 | $0.82 \pm 0.09$ | $0.82 \pm 0.02$ |
| 45 | $0.93 \pm 0.08$ | $0.93 \pm 0.02$ | 45 | $0.81 \pm 0.09$ | $0.81 \pm 0.02$ |
| 90 | $0.46 \pm 0.06$ | $0.46 \pm 0.01$ | 90 | $0.25 \pm 0.05$ | $0.25 \pm 0.01$ |
| **Predicted source angle** | **$24 \pm 26$°** | **$24 \pm 8$°** | **Predicted source angle** | **$23 \pm 12$°** | **$23 \pm 3$°** |

sample previously mentioned in Section 3.1. The hypothetical 0.5 kg sample of weapons grade Pu emits $3.6 \times 10^4$ n/s, and it was previously determined that the measurement would take 830 s in order to achieve $<15\%$ uncertainty in the 5 detectors between $-90°$ and 90°, resulting in $3 \times 10^7$ emitted neutrons. Previous experiments with the 0.13 mCi $^{252}$Cf source at the same position for 300 s provided detector responses corresponding $3.6 \times 10^8$ emitted fission neutrons. The internal detector responses of these experiments were scaled in order to calculate the same detector responses associated with the Pu sample, which emits $3 \times 10^7$ neutrons in the aforementioned timeframe. The absolute uncertainty of each detector was calculated using the scaled detector responses, which are depicted by the error bars in Fig. 12.

The shifted distributions in Fig. 12a and b show that the DSNDS is more sensitive to changes in the source position corresponding to the softer (moderated) neutron spectrum shown in Fig. 12b. Table 5 contains the simulated detector responses corresponding to the bare and moderated source configuration with uncertainties calculated for two source strengths. The data demonstrates that the angular resolution of the DSNDS is heavily dependent on the counting statistics of the individual detector responses.

The angular resolution of the DSNDS using the linear interpolation model, eight internal detectors with an angular spacing of 45°, and counting statistics corresponding to $3 \times 10^7$ emitted neutrons at a distance of 1.15 m from the DSNDS results in a prediction of the source angle with a relatively large uncertainty: $\pm 26°$ for a bare fission source and $\pm 12°$ for a fission moderated by 5 cm of HDPE. This resolution is low, but the measurement still provides useful information about the position of a hidden neutron source. Experimental results corresponding to $7.2 \times 10^8$ emitted neutrons at a distance of 1.15 m from the DSNDS result in an angular uncertainty of $\pm 8°$ and $\pm 3°$ for the bare and moderated source configurations, respectively. The angular resolution and overall efficiency of the system can be improved by the addition of more detectors with reduced angular spacing. The modularity of this design allows for the DSNDS to be improved in order to meet specific target criteria, e.g. efficiency and angular resolution.

## 4. Conclusions

The advancement of compact, solid-state thermal detectors has provided the opportunity to develop new applications related to neutron detection. The flat, compact devices developed at RPI operate with zero bias voltage, demonstrate scalability to large surface areas, have an intrinsic thermal neutron efficiency of ~29% at 0.0253 eV, and low gamma sensitivity [10]. The cost of each device in mass production is expected to be less than existing detectors, and because the detectors do not require bias for operation, the cost of the associated electronics is also reduced [24,25]. These characteristics have made possible the development of the presented modular DSNDS.

The DSNDS has demonstrated the ability to provide information about the location and energy of an unidentified, hidden neutron source. This information is in the form of the relative source angle, which narrows down the location of a neutron source. This angle may provide adequate information to locate the source; however, more information may be useful if the source is not exposed. In this case, the spectral information can be used to determine how heavily the source is moderated. The level of moderation can provide information related to the amount of moderating material covering the source. The DSNDS is sensitive to shielding with hydrogenous material and relatively insensitive to high-Z attenuation. The system can provide spectral information with as few as two detectors, but the system has a modular design allowing for increased detection efficiency and angular granularity at the expense of increased cost.

The DSNDS was designed for, but not limited to, the effort to survey shipping containers for diverted SNM. This system was tested with a reasonable source–detector distance of 1.15 m, but simulations demonstrate that the system can operate at as calibrated at distances greater than 1.0 m. Additionally, it was demonstrated that the DSNDS can provide a spectral and positional analysis of an unidentified neutron source in minutes—depending on the source strength, source-detector distance, and source attenuation. A quicker measurement can be made using a supplementary spectral analysis utilizing the internal-to-external detector response ratio. The DSNDS could reduce the time associated with the process of surveying containers for diverted SNM, reducing the unwanted economic effects of monitoring millions of shipping containers for SNM annually. Further development of the DSNDS should include an investigation of the system's effectiveness and time-requirements with variable source strengths and in environments with background neutron radiation.

## Acknowledgements

This work was supported by the U.S. Department of Homeland Security-Domestic Nuclear Detection Office (DNDO) under award nos. NSF/ECCS-1348269 and 2013-DN-077-ER0001. This support does not constitute an express or implied endorsement on the part of the Government.

## References

[1] U.S.N.R. Commission, Special Nuclear Material, [Online]. Available: ⟨http://www.nrc.gov/materials/sp-nucmaterials.html⟩.
[2] Office of Inspector General, United States Customs and Border Protection's Radiation Portal Monitors at Seaports. OIG-13-26, Department of Homeland Security, Washington, DC, January 2013.

[3] R. Kouzes, The He-3 Supply Problem (PNNL-18388), U.S. Department of Energy, Pacific Northwest National Laboratory, 2009.
[4] R.T. Kouzes, J.H. Ely, A.T. Lintereur, E.R. Siciliano, M.L. Woodring, BF3 Neutron Detector Tests( PNNL-19050), Pacific Northwest National Laboratory, 2009, December.
[5] J. Clinton, Optimization and Characterization of a Novel Self Powered Solid State Neutron Detector, Rensselaer Polytechnic Institute, Troy, NY, 2011, Ph.D. Thesis.
[6] D. McGregor, S. Bellinger, K. Shultis, Journal of Crystal Growth 379 (15) (2013) 99, September 2013.
[7] D. McGregor, S. Bellinger, W. McNeil, Materials Research Society Symposium (2009) 1164-L06-01.
[8] R. Nikolic, C. Cheung, C. Reinhardt, T. Wang, Future of Semiconductor Based Thermal Neutron Detectors (UCRL-PROC-219274), Lawrence Livermore National Lab, CA, USA, 2006, February.
[9] K. Huang, R. Dahal, N. LiCausi, J. Lu, Y. Danon, Journal of Vacuur Science and Technology B 30 (2012).
[10] K.-C. Huang, R. Dahal, J. Lu, A. Weltz, Y. Danon, I. Bhat, Nuclear Instruments and Methods in Physics Research A 763 (2014) 260–265.
[11] R. Kouzes, J. Ely, L. Erikson, W. Kernan, A. Lintereur, E. Siciliano, D. Stromswold, M. Woodring, Alternative Neutron Detection Testing Summary (PNNL-19311), Pacific Northwest National Laboratory, 2010.
[12] R. Schulte, M. Kesselman, Nuclear Instruments and Methods in Physics Research A (1999) 852.
[13] H. Yamanishi, Health Physics 38 (3) (2003) 267.
[14] A. Caruso, J. Petrosky, J. McClory, P. Dowben, W. Miller, T. Oakes, A. Bickley, Apparatus and Method for Directional and Spectral Analysis of Neutrons. US Patent 20120148004 A1, 14 June 2012.
[15] H. Yamanishi, Nuclear Instruments and Methods in Physics Research Section A: Accelerators, Spectrometers, Detectors and Associated Equipment 544 (3) (2005) 643.
[16] R.L. Bramblett, R.I. Ewing, T.W. Bonner, Nuclear Instruments and Methods 9 (1) (1960) 1.
[17] I.O. Braun, J. Andersson, A Neutron Rem Counter (AE-132), Aktiebolaget Atomenergy, Stockholm, Sweeden, 1964.
[18] J.W. Leake, Nuclear Instruments and Methods 45 (1) (1966) 151.
[19] C. Birattari, A. Esposito, A. Ferrari, M. Pelliccioni, R. Rancati, M. Silari, Radiation Protection and Dosimetry 76 (3) (1998) 135.
[20] C. Birattari, A. Ferrari, C. Nuccetelli, M. Pelliccioni, M. Silari, Nuclear Instruments and Methods A 297 (1-2) (1990) 250.
[21] S.D. Monk, M.J. Joyce, Z. Jarrah, D. King, M. Oppenheim, Review of Scientific Instruments 79 (1) (2008).
[22] J. Goorley et al., Initial MCNP6 Release Overview—MCNP6 version 1.0 LA-UR-13-22934, 2013.
[23] R.B. Firestone, Table of Isotopes, eighth ed., Lawrence Berkeley National Laboratory, University of California: John Wiley & Sons, Inc., 1996.
[24] K.-C. Huang, R. Dahal, N. LiCausi, J. Lu, Journal of Vacuum Science and Technology, B 20 (5) (2012).
[25] K.-C. Huang, R. Dahal, J. Lu, Y. Danon, I. Bhat, Applied Physics Letters 102 (2013).